Research Square

Preprints are preliminary reports that have not undergone peer review.
They should not be considered conclusive, used to inform clinical practice,
or referenced by the media as validated information.

Solvent-Mediated Structural, Optical and Ammonia-Sensing Characteristics of Spray-Pyrolysed Nickel Ferrite ($NiFe_2O_4$) Thin Films

C. S.A. Raj

csaraj.aac@gmail.com

Arul Anandar College (Autonomous)

Research Article

Keywords: nickel ferrite, $NiFe_2O_4$, spray pyrolysis, solvent engineering, optical band gap, ammonia sensing, spinel ferrite

Posted Date: October 28th, 2026

DOI: https://doi.org/10.21203/rs.3.rs-11507422/v1

License: This work is licensed under a Creative Commons Attribution 4.0 International License.
Read Full License

Additional Declarations: The authors declare no competing interests.

Abstract

Solvent selection can exert a substantial influence on the microstructural development and functional response of oxide thin films prepared by aerosol-based deposition. In this study, nickel ferrite ($NiFe_2O_4$) thin films were deposited on glass substrates by nebulizer-assisted spray pyrolysis using water, methanol, ethanol and isopropanol-containing precursor solutions. The resulting films were examined by X-ray diffraction (XRD), scanning electron microscopy (SEM), UV–visible spectroscopy and ammonia (NH_3) sensing measurements. XRD analysis was reported to be consistent with a cubic spinel structure, while the ethanol-containing formulation produced the sharpest diffraction peaks and the largest estimated crystallite size (approximately 24.5 nm). SEM observations indicated a comparatively uniform, porous and less agglomerated surface for the ethanol-derived film. Optical analysis yielded an estimated band gap of approximately 1.86 eV for this sample, lower than the values reported for the water-, methanol- and isopropanol-derived films. The ethanol-derived film also exhibited a concentration-dependent current response to NH_3, with a reported response of approximately 500% at 250 ppm. These findings suggest that solvent composition is a potentially useful processing variable for tailoring the structural, optical and gas-sensing behaviour of spray-pyrolysed $NiFe_2O_4$ films. Further quantitative validation—including replicate measurements, response and recovery times, selectivity, baseline stability and uncertainty analysis—is required before practical sensor performance can be established.

1 Introduction

Functional oxide thin films are widely investigated because their electrical, optical, chemical and magnetic responses can be adjusted through composition, microstructure and processing conditions. Their relatively large surface-to-volume ratios and compatibility with compact device architectures make them relevant to sensing, optoelectronics, catalysis, energy technologies and selected magnetic applications [1, 2]. The performance of a thin-film device, however, depends not only on its nominal composition but also on crystallinity, grain size, porosity, defect populations, film continuity and the interfaces formed during deposition.

Spinel ferrites, generally represented as MFe_2O_4, constitute a versatile class of transition-metal oxides in which magnetic ordering and semiconducting behaviour coexist. Their properties depend on the divalent cation, cation distribution between tetrahedral and octahedral sites, microstructure and synthesis history [3, 4, 9]. Nickel ferrite ($NiFe_2O_4$), commonly described as an inverse-spinel ferrite, is of particular interest because of its chemical and thermal stability, ferrimagnetic behaviour and relatively high electrical resistivity. These characteristics have motivated research into magnetic components, catalytic systems and chemical sensors.

Gas sensors based on semiconducting metal oxides are important for monitoring industrial processes, indoor air quality and environmental hazards. Their operation commonly involves a change in electrical resistance or current as gas molecules interact with adsorbed oxygen species and surface-active sites. The magnitude and kinetics of the response depend on temperature, target-gas concentration, oxygen

availability, grain boundaries, porosity and the electronic properties of the sensing layer [7, 8, 10–14]. For this reason, sensor optimisation requires attention to both material chemistry and the microstructure generated during fabrication.

Spray pyrolysis is an accessible route for depositing oxide films over comparatively large areas. A precursor solution is atomised into droplets, transported to a heated substrate and converted through solvent evaporation and precursor decomposition. The final film can be influenced by substrate temperature, precursor concentration, spray rate, carrier-gas conditions, nozzle-to-substrate distance and solvent properties [18, 19]. Solvent composition may affect droplet size, wetting, evaporation, solute transport and the sequence of nucleation and grain growth. Accordingly, solvent selection offers a practical means of modifying film morphology without deliberately changing the target oxide composition.

Although nickel ferrite has been investigated for magnetic and sensing applications, the relationship between solvent composition, film microstructure, optical absorption and ammonia response warrants careful evaluation under controlled conditions. The present work compares $NiFe_2O_4$ films prepared using water, water–methanol, water–ethanol and water–isopropanol precursor media. The films were characterised using XRD, SEM and UV–visible spectroscopy, and their current response to ammonia was measured. The principal objective is to assess whether solvent choice is associated with systematic differences in the measured properties. The interpretation is restricted to the evidence reported here; proposed explanations involving surface area, defect density and charge transport should be considered hypotheses unless independently quantified.

2 Materials and methods

2.1 Precursor preparation and film deposition

Nickel chloride and ferric chloride were used as precursor salts. Four solvent formulations were reported: 10 mL water; 8 mL water with 2 mL methanol; 8 mL water with 2 mL ethanol; and 8 mL water with 2 mL isopropanol. The precursor solutions were deposited onto glass substrates using a nebulizer-assisted spray-pyrolysis arrangement. The substrate temperature was maintained at 450°C, the spray pressure was reported as 1.5 kg cm^{-2}, and the nozzle-to-substrate distance was 5 cm.

After deposition, the films were annealed at 600°C for 24 h. Because precursor concentrations, total solution volumes used per sample, spray duration, solution flow rate and number of replicate depositions are not specified in the supplied manuscript, these details should be added from laboratory records before submission. The precursor stoichiometry and any post-deposition mass loss should also be documented so that the preparation can be reproduced.

2.2 Structural, morphological and optical characterisation

X-ray diffraction patterns were recorded using a Bruker D8 Advance diffractometer with Cu Kα radiation (λ = 1.5406 Å), over a reported 2θ range of 10°–80° at a scan rate of 2° min^{-1}. Surface morphology was examined by scanning electron microscopy. Optical measurements were performed using a Shimadzu UV-2600 UV–visible spectrophotometer over the reported wavelength range of 400–1000 nm. The optical band gap was estimated from Tauc analysis. For reproducible analysis, the manuscript should specify the assumed transition type, the transformation used, the fitting interval and the method used to determine the absorption coefficient.

2.3 Ammonia-sensing measurements

The electrical response was monitored using a Keithley 2450 source meter, with silver paste used to form contacts. The supplied description indicates that samples were placed in a metal-tube chamber equipped with a heating coil and thermocouple. Ammonia vapour was generated by heating an ammonia solution, and the chamber was evacuated after each measurement. Measurements were reported across a concentration range extending from 25 to 250 ppm in the manuscript's different sections; the exact concentrations used in each experiment must be reconciled and explicitly listed in the final version.

The reported response was calculated as $S(\%) = [(I_g - I_a)/I_a] \times 100$, where I_a is the current measured in air and I_g is the current during NH_3 exposure. With the stated current values of approximately 1.0×10^{-6} A in air and 6.0×10^{-6} A under 250 ppm NH_3, this expression gives 500%. The test temperature, gas-flow or chamber-pressure conditions, exposure duration, recovery protocol, number of repeated cycles, calibration procedure and uncertainty should be supplied to support quantitative comparison with other sensors.

3 Results and discussion

3.1 Crystal structure and microstructural indicators

The reported diffraction patterns were indexed to reflections assigned to cubic spinel $NiFe_2O_4$, including (111), (220), (311), (400), (331), (422), (511) and (440). The (311) peak positions were reported between 35.55° and 35.58° for the four solvent formulations. The ethanol-derived sample showed the narrowest reported full width at half maximum (0.34°) and the largest Scherrer-estimated crystallite size (24.5 nm), compared with 16.0 nm for the water-derived sample. The estimated lattice parameter was approximately 8.34 Å for all samples.

These results are consistent with a solvent-associated change in the coherent diffraction domain size and peak broadening. The Scherrer estimate, however, is not necessarily equivalent to the physical grain size observed by SEM; instrumental broadening, microstrain and overlapping reflections can influence peak widths. The manuscript should state whether instrumental broadening was corrected and provide the calculation details. In addition, the assertion of phase purity should be supported by the complete

diffraction patterns and, where possible, comparison with an appropriate reference pattern rather than peak assignments alone.

Table 1
Reported structural parameters of $NiFe_2O_4$ films prepared using different solvent formulations.

Solvent	2θ (311) (°)	FWHM (°)	D (nm)	δ (×10⁻⁴ nm⁻²)	ε (×10⁻³)
Water	35.55	0.52	16.0	3.91	6.8
Methanol-containing	35.57	0.48	17.3	3.34	6.3
Ethanol-containing	35.58	0.34	24.5	1.67	4.5
Isopropanol-containing	35.56	0.44	18.9	2.80	5.8

The tabulated dislocation-density and strain values are reproduced from the supplied manuscript and should be recalculated or verified against the stated equations and units before publication. The relationship between solvent properties and crystallisation should also be framed cautiously: solvent polarity alone is insufficient to establish a mechanism without measurements or a more complete account of evaporation, wetting, precursor chemistry and deposition dynamics.

3.2 Surface morphology

The supplied SEM interpretation describes the water-derived film as relatively dense and agglomerated, with irregularly shaped particles, whereas the ethanol-containing film is described as more uniform and porous, with reduced agglomeration. This qualitative difference is consistent with the XRD-derived indication of a larger coherent diffraction domain for the ethanol-containing sample. Nevertheless, qualitative SEM images do not by themselves establish a larger specific surface area or a lower defect density. Such claims would require quantitative image analysis, suitable surface-area measurements or complementary characterisation.

From a sensing perspective, a porous morphology may increase the fraction of accessible surface sites and shorten diffusion paths, while grain boundaries and surface defects can influence carrier transport. These are plausible mechanisms, but their relative contributions cannot be separated from the present evidence. A stronger analysis would quantify grain-size distributions and porosity from multiple representative fields and relate those metrics to sensor response across all four formulations.

3.3 Optical response and estimated band gap

The UV–visible results indicate solvent-dependent optical absorption. The reported Tauc-derived band gaps were approximately 2.20 eV for the water-derived film, 2.15 eV for the methanol-containing film, 1.86 eV for the ethanol-containing film and 2.86 eV for the isopropanol-containing film. The ethanol-derived sample therefore had the lowest reported estimated band gap and was described as exhibiting a red-shifted absorption edge.

These values should be interpreted as estimates that depend on the optical model and data treatment. For semiconducting ferrites, the assumed transition type and the choice of linear fitting region can materially affect a Tauc extrapolation. The final manuscript should show the underlying spectra and Tauc plots, specify the transition exponent and fitting interval, and explain how reflectance, scattering and film thickness were handled. Improved crystallinity may contribute to optical differences, but it should not be presented as the sole cause without evidence that distinguishes crystallinity from defect chemistry, cation distribution, thickness and other variables.

3.4 Ammonia-sensing response

The ethanol-containing $NiFe_2O_4$ film exhibited an increase in current during NH_3 exposure, and the reported response increased with gas concentration. At 250 ppm, the current was reported to rise from approximately 1.0×10^{-6} A in air to 6.0×10^{-6} A in the presence of ammonia. Applying the stated response equation yields a response of 500%. This is a substantial relative current change under the reported conditions, although the absolute value alone does not establish selectivity, detection limit, response speed, recovery, repeatability or long-term reliability.

The manuscript currently gives different concentration ranges in different sections: the experimental description mentions 25–150 ppm, whereas the results and abstract include measurements up to 250 ppm. This discrepancy must be resolved using the original laboratory records. The description of generating ammonia vapour by heating an ammonia solution also requires a clear account of concentration calibration and gas delivery. For a rigorous sensor study, the authors should report controlled NH_3 concentrations, operating temperature, humidity, exposure and purge durations, repeated response cycles, baseline drift, and responses to relevant interfering gases. Without these data, claims of high-performance practical sensing should remain provisional.

The proposed link between the ethanol-containing formulation and the higher response is plausible: differences in surface morphology, grain boundaries and charge transport may alter adsorption and electrical transduction. However, the current data do not establish which mechanism dominates. Surface-chemical analysis, impedance measurements, controlled temperature-dependent sensing or other complementary methods could help distinguish these possibilities.

4 Conclusions

$NiFe_2O_4$ thin films were prepared by nebulizer-assisted spray pyrolysis using water, methanol-, ethanol- and isopropanol-containing precursor media. The reported results indicate that solvent formulation is associated with differences in diffraction peak width, estimated crystallite size, surface morphology, optical band gap and current response to ammonia. Among the investigated samples, the ethanol-containing formulation exhibited the narrowest reported diffraction peak, the largest estimated crystallite size (approximately 24.5 nm), the lowest reported optical band gap (approximately 1.86 eV) and a reported NH_3 response of approximately 500% at 250 ppm. These observations identify solvent composition as a potentially useful processing variable for $NiFe_2O_4$ thin films. However, the mechanisms

linking solvent properties to film growth and sensing remain to be demonstrated directly, and practical sensor performance cannot be fully assessed without reproducibility, selectivity, response/recovery, stability and uncertainty data. Biomedical applications such as MRI contrast enhancement, magnetic drug delivery and magnetic hyperthermia are not demonstrated by the present experiments and should be discussed only as prospective research directions requiring independent magnetic, toxicological and biological evaluation.

Declarations

Funding: No

Competing interests: No

Author contributions: C. S. A. Raj developed the study, conducted the experimental work and prepared the manuscript.

References

1. Chopra, K. L. Thin Film Phenomena. McGraw-Hill, New York (1969).
2. Maissel, L. I. & Glang, R. (eds.) Handbook of Thin Film Technology. McGraw-Hill, New York (1970).
3. Goldman, A. Modern Ferrite Technology, 2nd edn. Springer, New York (2006).
4. Smit, J. & Wijn, H. P. J. Ferrites: Physical Properties of Ferrimagnetic Oxides in Relation to Their Technical Applications. Philips Technical Library, Eindhoven (1959).
5. Pullar, R. C. Hexagonal ferrites: a review of the synthesis, properties and applications of hexaferrite ceramics. Prog. Mater. Sci. 57, 1191–1334 (2012).
6. Özgür, Ü. et al. A comprehensive review of ZnO materials and devices. J. Appl. Phys. 98, 041301 (2005).
7. Barsan, N. & Weimar, U. Conduction model of metal oxide gas sensors. J. Electroceram. 7, 143–167 (2001).
8. Yamazoe, N. & Miura, N. Environmental gas sensing. Sens. Actuators B Chem. 20, 95–102 (1994).
9. Rao, C. N. R. & Raveau, B. (eds.) Transition Metal Oxides: Structure, Properties and Synthesis of Ceramic Oxides, 2nd edn. Wiley-VCH, Weinheim (1998).
10. Korotcenkov, G. Handbook of Gas Sensor Materials: Properties, Advantages and Shortcomings for Applications, Vol. 1. Springer, New York (2013).
11. Korotcenkov, G. Metal oxides for solid-state gas sensors: what determines our choice? Mater. Sci. Eng. B 139, 1–23 (2007).
12. Barsan, N., Koziej, D. & Weimar, U. Metal oxide-based gas sensor research: how to? Sens. Actuators B Chem. 121, 18–35 (2007).

13. Wang, C., Yin, L., Zhang, L., Xiang, D. & Gao, R. Metal oxide gas sensors: sensitivity and influencing factors. Sensors 10, 2088–2106 (2010).
14. Moseley, P. T. Solid state gas sensors. Meas. Sci. Technol. 8, 223–237 (1997).
15. Faglia, G., Sberveglieri, G., Depero, L. & Groppelli, G. Gas sensing properties of nanocrystalline metal oxide thin films. Sens. Actuators B Chem. 23, 161–166 (1995).
16. Murugan, R., Kalaivani, K. & Manimozhi, V. Structural, optical and magnetic properties of spray pyrolyzed nickel ferrite thin films. J. Mater. Sci. Mater. Electron. 27, 3680–3688 (2016). Verify this reference against the publisher record before submission.
17. Sutka, A. & Gross, K. A. Spin spray deposition of ferrite films: a review. Sens. Actuators A Phys. 187, 95–105 (2012).
18. Kale, R. B., Lokhande, C. D. & Han, S. H. Spray pyrolysis deposition of metal oxide thin films: a review. Mater. Chem. Phys. 82, 680–688 (2003).
19. Patil, P. S. Versatility of chemical spray pyrolysis technique. Mater. Chem. Phys. 59, 185–198 (1999).
20. Shannon, R. D. Revised effective ionic radii and systematic studies of interatomic distances in halides and chalcogenides. Acta Crystallogr. A 32, 751–767 (1976).
21. Gubin, S. P. et al. Magnetic nanoparticles: preparation, structure and properties. J. Magn. Magn. Mater. (2009). Complete volume and page details before submission.
22. Laurent, S. et al. Magnetic iron oxide nanoparticles: synthesis, stabilization, vectorization, physicochemical characterizations, and biological applications. Mater. Sci. Eng. C (2012). Complete volume and page details before submission.

Figures

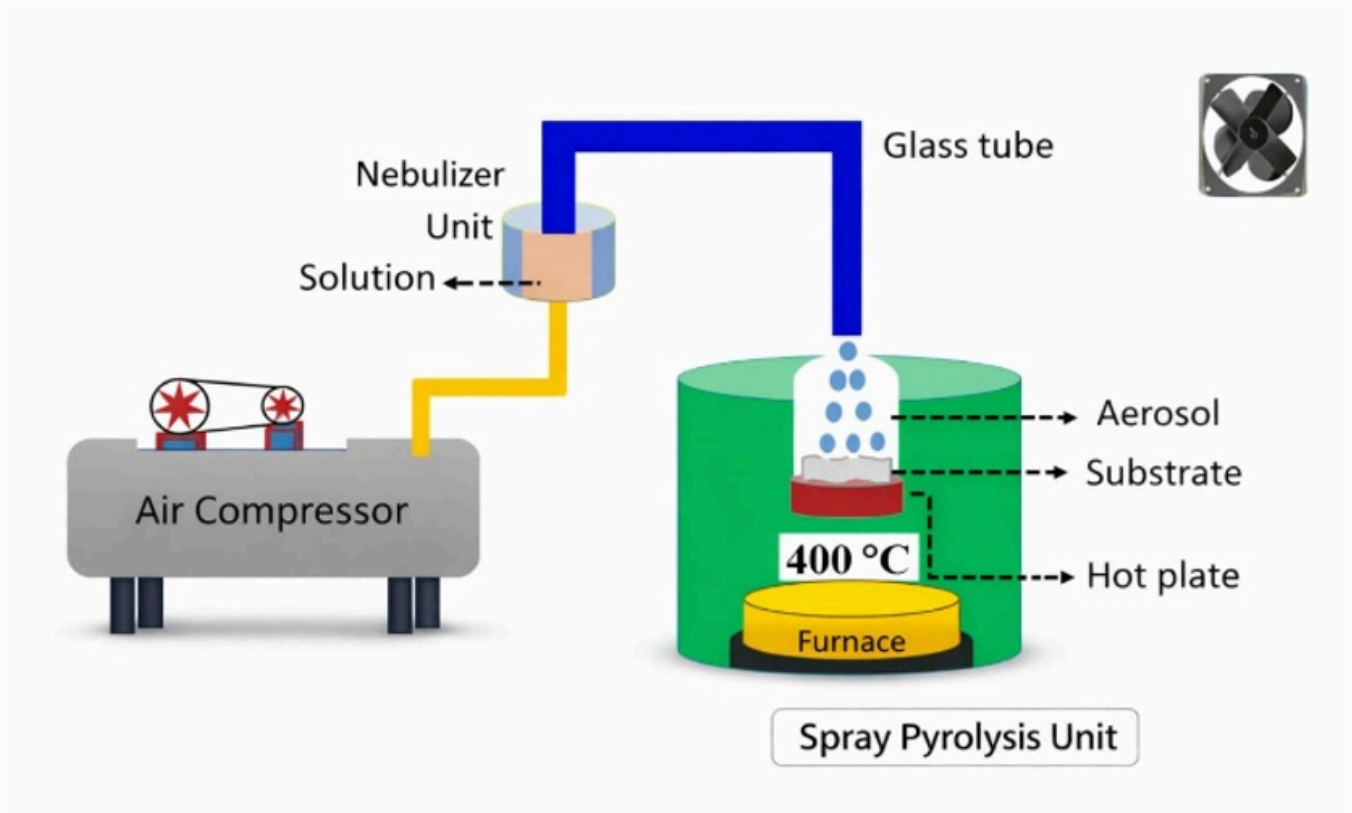


Figure 1

Schematic representation of the nebulizer-assisted spray-pyrolysis arrangement used for $NiFe_2O_4$ thin-film deposition. The source figure labels a substrate-heating temperature of 400 °C, whereas the manuscript text reports 450 °C; reconcile this discrepancy before submission.

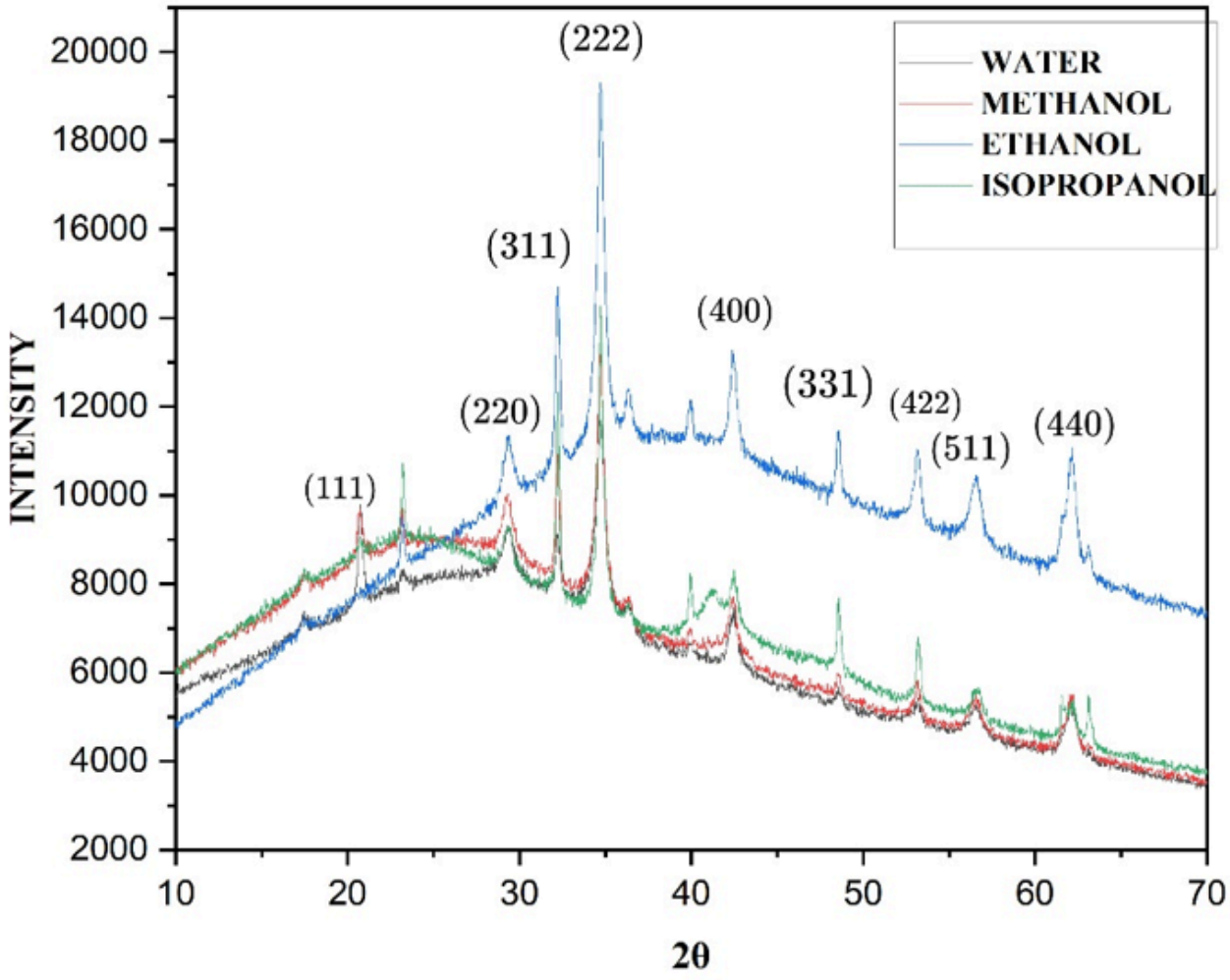


Figure 2

X-ray diffraction patterns of $NiFe_2O_4$ thin films prepared using water, methanol, ethanol and isopropanol as solvent media. Reproduced from the uploaded source manuscript.

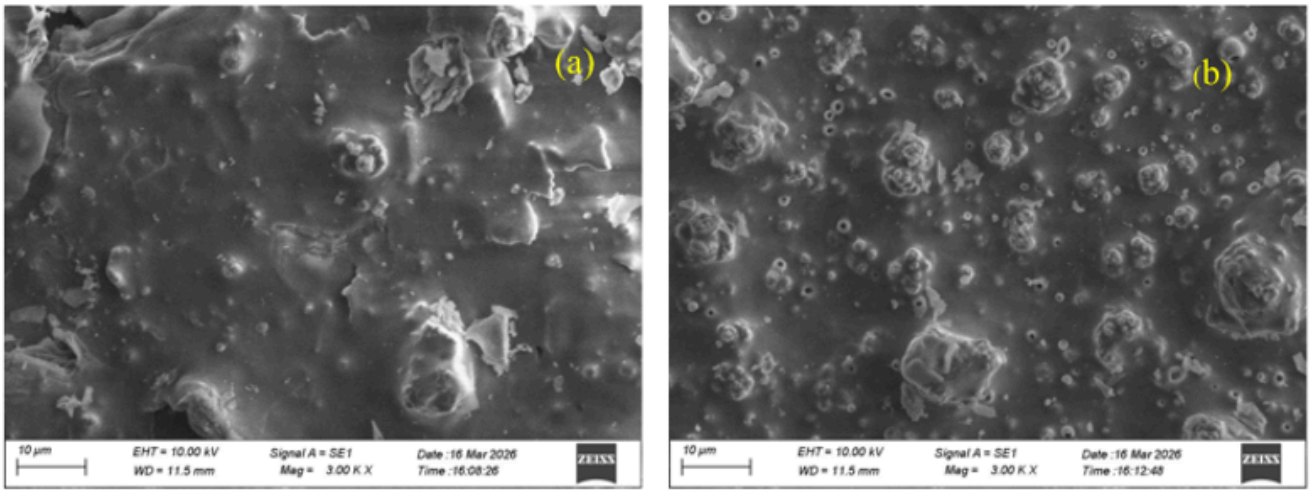


Fig 5.2.SEM IMAGE OF a) WATER b) ETHANOL OF NiFe2O4

Figure 3

SEM micrographs of $NiFe_2O_4$ thin films prepared using (a) water and (b) ethanol. Original micrographs and embedded scale information are retained from the source file.

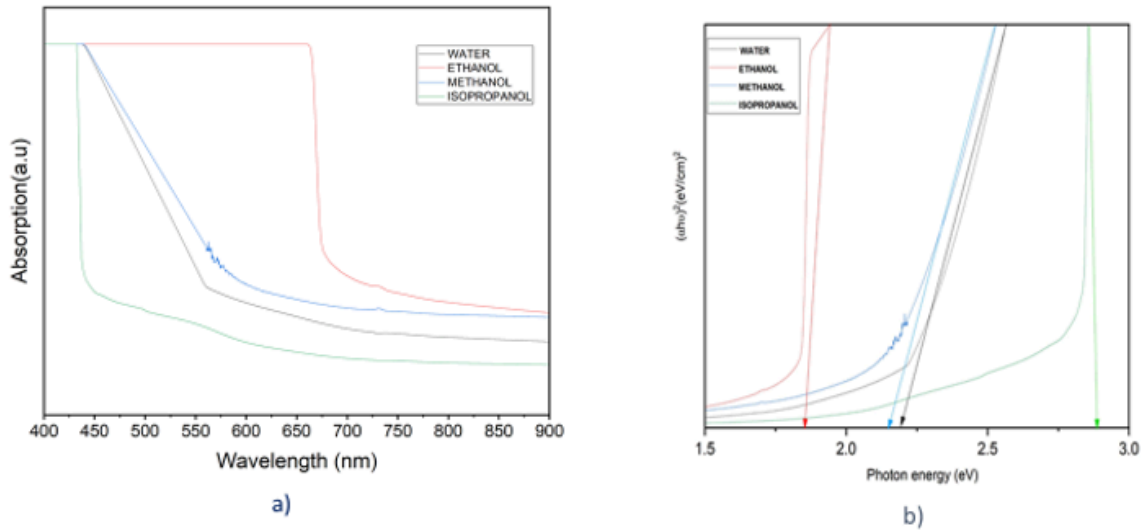


Fig 5.3 a)Absorbance of NiFe2O4 for various solvents b)Tauc plot

Figure 4

(a) UV–visible absorbance spectra and (b) Tauc plots for $NiFe_2O_4$ thin films prepared using different solvent formulations. Verify the reported band-gap values against the original spectra and fitting procedure.

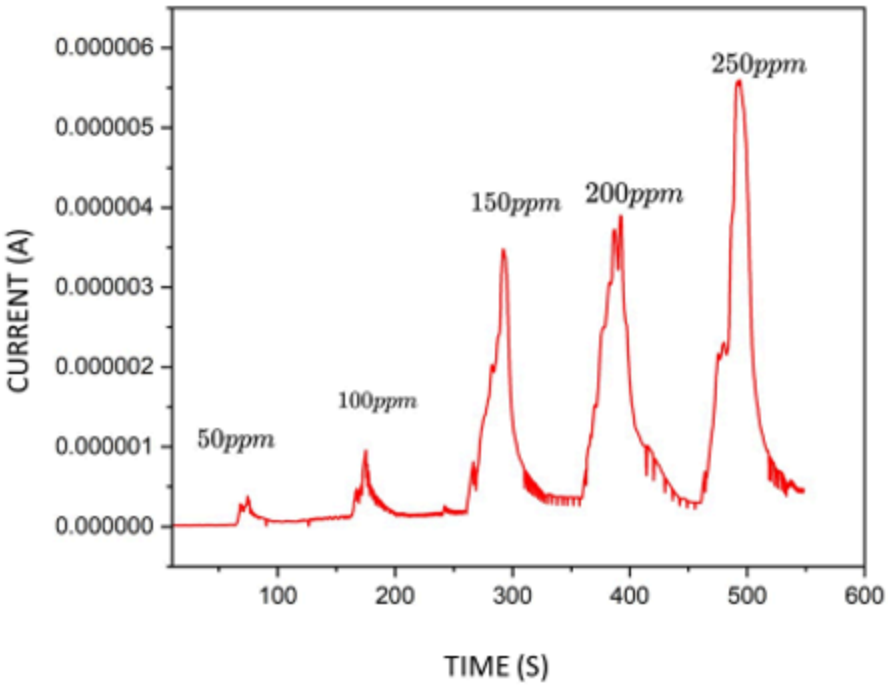


FIG 5.4 Indicates the gas sensing response between the Time(s) Vs current (A)

Figure 5

Current-versus-time response of the $NiFe_2O_4$ film during ammonia exposures at concentrations annotated in the original plot. The source graph includes labels up to 250 ppm; reconcile this with the 25–150 ppm range stated in the methods.